Proc. Natl. Acad. Sci. USA
Vol. 90, pp. 93–97, January 1994
Neurobiology

Techniques for measuring sulcal/gyral patterns in the brain as visualized through magnetic resonance scanning: BRAINPLOT and BRAINMAP

(neuroanatomy/brain development/Alzheimer disease/cognition)

NANCY C. ANDREASEN*†‡, GREG HARRIS*, TED CIZADLO*, STEPHAN ARNDT*, DANIEL S. O'LEARY*, VICTOR SWAYZE*†, AND MICHAEL FLAUM*†

*Mental Health Clinical Research Center and †the Department of Psychiatry, College of Medicine, University of Iowa Hospitals and Clinics, 200 Hawkins Drive, Iowa City, IA 52242

Communicated by Patricia Goldman-Rakic, August 9, 1993 (received for review March 6, 1993)

ABSTRACT **A method for measuring sulcal and gyral patterns, using data derived from magnetic resonance (MR) scanning, is described. This method can be applied through two newly developed computer programs, BRAINPLOT and BRAINMAP. These programs provide quantitative measures of brain surface pattern. The method has been validated with postmortem brains, phantoms, and human MR data. The method is robust to detecting differences in brain surface anatomy between atrophic and nonatrophic brains. It appears to offer an efficient, fully automated, and accurate method for analyzing the large amounts of information generated through *in vivo* neuroimaging techniques.**

The development of *in vivo* brain imaging techniques has provided neuroscientists with unprecedented opportunities for studying structure/function relationships in the human brain. In particular, magnetic resonance (MR) scanning permits the study of aspects of neuroanatomy that have been hitherto difficult when resources are limited to postmortem tissue. Because it is noninvasive, MR can be used to study large samples. In addition, it can be applied to the study of individuals of all ages, thereby eliminating confounds that occur as a consequence of the aging process (1–4). Finally, MR is superbly adapted to the study of three-dimensional neuroanatomy, since it permits visualization and resampling in multiple planes simultaneously.

Recent developments in MR data acquisition have enhanced the capacity to study three-dimensional brain surface anatomy. High-speed three-dimensional acquisition techniques now permit investigators to obtain data in very thin slices (e.g., 1–1.5 mm), providing a data set consisting of near-cubic voxels. Consequently, MR data sets are now well adapted to the application of surface/volume rendering techniques, which permit excellent visualization of sulcal/gyral anatomy of the brain surface, as well as high-resolution resampling and visualization of internal brain structures (5–12).

The wealth of information produced through these advances in MR technology presents particular challenges for analyzing the large quantities of information that can be generated. This report addresses one specific issue: techniques for measuring the surface pattern and complexity of sulci and gyri. It describes the development of a method that provides quantitative estimates of various aspects of the brain surface that reflect sulcal/gyral patterns, such as degree of concavity, convexity, or overall variability.

Obtaining summary measures of sulcal and gyral anatomy of the human brain can potentially provide important information concerning brain development and a variety of disease processes. Sulcal and gyral patterns reflect brain maturational processes and may contain clues concerning the relationship between brain maturation and the development of specific mental abilities in healthy normal individuals, as well as the effects of abnormalities in development due to either genetic or environmental factors. The formation of sulcal and gyral patterns in the brain appears to be a genetically programmed event, which may be partially modified by environmental influences such as general health, nutrition, and injury. The surface of the brain is essentially smooth until the sixth month of gestation, and thereafter the complex enfolding that characterizes the adult human brain begins to occur. The major sulci (e.g., sylvian fissure, central sulcus) form during the sixth and seventh months of fetal life and continue to develop throughout the gestational period and after birth (13). The pattern of enfolding is an effect of the massive expansion of cortical grey matter and the development of interconnecting circuits. The extent to which these events are genetically programmed versus environmentally influenced is at present unknown. Information about individual differences in sulcal/gyral patterns may ultimately be informative about brain plasticity and the effects of environmental stimuli or injuries on brain growth and development (14–16).

Because large samples of normal and diseased human brains were not widely available for study prior to the advent of MR scanning, we at present know very little about normal variations in sulcal/gyral anatomy. The largest atlas available to date is based on only 25 brains of unknown age and gender (12). Summary information concerning sulcal and gyral patterns in that atlas depends on visual description and manual tracing. The primary technique used by neuroanatomists to study brain variation has involved stereology, which depends on manual slicing and tracing and is quite labor intensive (17–21). Even computer-based techniques developed to date, such as BRAINPRINT, are extremely time consuming (22).

A more efficient technique for measuring sulcal/gyral anatomy is clearly needed. We report here on a simple yet sensitive automated technique that provides quantitative data. This technique is implemented through two image-analysis programs, BRAINPLOT and BRAINMAP. The two programs provide a statistical estimate of surface pattern and complexity (BRAINPLOT) and a surface map that is based on the detailed numeric data concerning surface patterns (BRAINMAP).

METHODS

MR Scanning Sequence. MR data are collected using a 1.5-T GE Signa Scanner. The spoiled grass sequence is used with the following scanning parameters: 1.5-mm coronal

The publication costs of this article were defrayed in part by page charge payment. This article must therefore be hereby marked "*advertisement*" in accordance with 18 U.S.C. §1734 solely to indicate this fact.

Abbreviation: MR, magnetic resonance.

‡To whom reprint requests should be addressed.

slices; flip angle, 40°; repetition time, 24 msec; echo time, 5 msec; two excitations; field of view, 26 cm; matrix, 256 × 192. This sequence yields ≈124 contiguous slices through the entire brain and requires an acquisition time of ≈20 min. Acquisition time can be halved if excitations are reduced to 1, with some loss in image quality.

Postacquisition Image Processing. Postacquisition processing is done using locally developed software. After acquisition, the MR data are converted to a three-dimensional data set using BRAINBLAST, a voxel processing program that does surface and volume rendering (23–25). The brain is initially "cut out" of the skull by using edge detection techniques and manual tracing; this is the most labor-intensive part of the analysis, usually requiring ≈2 hr for a 124-slice image set; the remainder of the method is totally automated. After this step, the pixels representing cerebrospinal fluid are "washed off" using a threshold based on training classes and histograms. The remaining pixels comprise a data set that provides a visualization and mask of the brain surface. This surface mask is then analyzed with the two programs described here, BRAINPLOT and BRAINMAP. BRAINBLAST performs a variety of other functions, such as object rotation and resampling with simultaneous visualization in multiple planes. It has the limitations in its capacity for surface visualization and object rotation that are inherent in methods that use lighting models (6, 7, 9, 11, 12).

Conceptualization of BRAINPLOT and BRAINMAP. BRAINPLOT and BRAINMAP have been developed in order to provide measures of the shape of brain surface patterns. The BRAINPLOT procedure provides a method for quantifying sulcal and gyral surface patterns for an individual brain or brain subregion. Subregions (e.g., frontal lobes, cerebellum) can be delineated by identifying sulcal landmarks using coordinates from a standard atlas (26).

The first step in the BRAINPLOT procedure quantifies the degree of concavity or convexity of each point on the cortical surface. This is accomplished in an automated manner by surveying the local environment of each surface voxel, leading to the assignment of a "curvature index" to each individual voxel. The curvature index reflects the relative position of that voxel in relation to surrounding voxels. The curvature index has positive, negative, and zero values. Positive values represent convexity, negative values represent concavity, and zero values represent flatness. The survey of the environment occurs three-dimensionally, encompassing coronal, sagittal, and transaxial planes.

A surface voxel has between 4 and 8 vertices exposed to the surface. For example, if the voxel is in the center of a plane, 4 vertices are exposed (Fig. 1 *Left*); if it is sticking out of the plane, 8 vertices are exposed (Fig. 1 *Right*). Since the survey of the surface occurs in three dimensions, and since individual voxels have a variable number of vertices exposed, between 8 and 24 curvature indices may be calculated for any given voxel. In Fig. 1 *Left*, where the voxel is part of a flat surface and only has two dimensions, eight vertices are found. In Fig. 1 *Right*, where the voxel protrudes from the surface, all three dimensions are needed to describe the voxel, and 20 vertices are present. In the case (not shown) of a voxel connected to the surface by only one corner, 24 vertices would be present.

The curvature index is based on vectors between the vertices of adjacent voxels and the vertex of an individual voxel (Fig. 2, point *a*); it is found by drawing a line between the endpoints of the vectors from the vertices of adjacent voxels (points *b* and *c*). The cross-product of the two vectors **ab** and **ac** determines the sign of the curvature index (positive = a convex surface; negative = a concave surface), and the magnitude of the curvature index is the length of the line found with the Pythagorean theorem.

The measure is calculated for each vertex j in a particular dimension k by

$$C_{jk} = \frac{\mathbf{ab} \times \mathbf{ac}}{|\mathbf{ab} \times \mathbf{ac}|} \left(2f - \sqrt{(b_x - c_x)^2 + (b_y - c_y)^2 + (b_z - c_z)^2} \right), \quad [1]$$

where **ab** × **ac** is the cross-product between vectors **ab** and **ac** and f is the distance between a and c and between a and b. The choice of f (or "filter") can be as small as 1, or a larger value can be assigned. A larger value of f will tend to smooth the surface and will therefore be more desirable for producing an image of the output (see discussion of BRAINMAP below). A value of 4 was chosen to generate Fig. 4, which illustrates the application of these programs for visualization. A value of 2 was used for statistical comparisons to determine whether the method could detect differences between atrophic and nonatrophic brains. A discussion of the theoretical and empirical reasons for selecting a particular filter will be presented in a subsequent publication.

The curvature indices for all vertices of voxels on the surface of the brain as a whole (or a specifically designated brain region) are calculated; these indices form a unique distribution. The surface features of the brain or subregions can be characterized by using the four statistical moments of the distribution. The four statistical moments (i.e., centeredness, variance, skewness, and kurtosis) provide a description of the unique distribution and hence patterns of sulcal and gyral morphology.

Fig. 3 illustrates examples of the variations in sulcal/gyral patterns that BRAINPLOT was designed to measure. For example, it could be postulated that in a healthy normal brain the majority of the curvature indices would be positive, reflecting the gentle convexity of healthy gyri, along with a smaller number of highly negative values, representing the sharply concave invagination of sulci. In contrast, an aging or atrophic brain, in which the sulci become wider and deeper and the gyri become narrow and shrunken, should be described by a different distribution of curvature indices. One might expect a more equal distribution of concave and convex points, resulting in a lower mean (moment one). As illustrated in Fig. 3, the variance, skewness, and kurtosis of this distribution might also be expected to be lower in an atrophic brain surface when compared to a normal one. The moments of these distributions could also discriminate characteristic sulcal and gyral patterns in other groups of individuals (e.g., males vs. females) or within subjects for

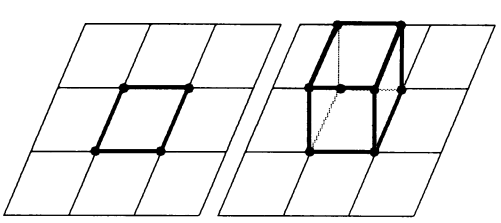

FIG. 1. Schematic showing how the number of vertices used to calculate curvature indices may vary.

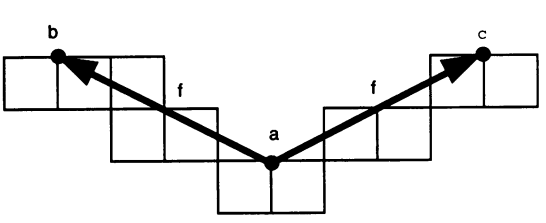

FIG. 2. Schematic showing vectors used to calculate curvature indices.

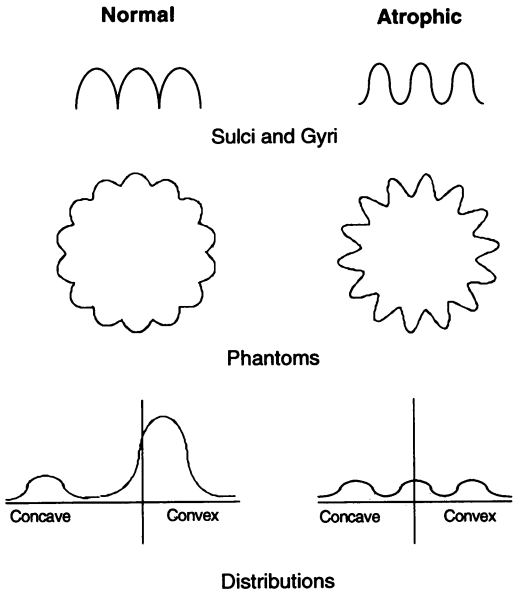

FIG. 3. Schematic showing hypothesized differences between a section of the surface of a normal brain (*Left*) and an atrophic brain (*Right*). Normal brain has rounded and full gyri and small sulci; atrophic brain has larger and deeper sulci (top row). "Cookie cutter" phantoms were generated, using simple mathematical functions, to simulate these surface shapes (middle row); curvature indices were calculated for these phantoms and were observed to differ significantly, suggesting that the method is sensitive to differences in brain surface shape. Theoretical distributions of the moments that would be generated by normal and atrophic brains are also shown (bottom row). Normal brain surface should be mostly convex, with a few areas that are highly concave, while the atrophic surface should be more equally concave and convex. The moments should reflect these differences, with normal brains having greater values for all four moments (i.e., a greater mean, variance, skewness, and kurtosis).

specific brain subregions (e.g., frontal versus occipital cortex).

BRAINMAP provides complementary data in a companion utility. As indicated in Eq. 2, the curvature indices calculated through Eq. 1 produce an average curvature index (C_a) that describes each voxel three-dimensionally.

$$C_a = \sum_j \sum_k \frac{C_{jk}}{n_a}, \qquad [2]$$

where n_a is the total number of j vertices in all k dimensions.

These values are assigned a grey scale number, based on their direction and magnitude, which can then be used to generate a visual display, or BRAINMAP, which depicts the sulci and gyri on the surface of the brain. Darker shades of grey are assigned to the negative values, which represent sulci, while lighter shades are assigned to positive values, which represent gyri. In addition, BRAINMAP also provides an estimate of the number of curvature indices that are positive (convex) and negative (concave), which provides additional descriptors of surface pattern.

The output from BRAINMAP has two components. One is an image that is based on combining the average curvature indices generated for each voxel with spatial location information (see Fig. 4). Since the image produced by BRAINMAP can be visually inspected and rotated, it provides a check on the face validity of BRAINPLOT. The availability of the combined curvature indices and spatial location information also permits mapping onto a normalized brain, as in the Talairach *Atlas* space (26). The second component of BRAINMAP consists of numeric data that define characteristics of the brain surface. These include the number of values of C_a that are greater than or less than the expected curvature (i.e., number of positive and negative C_a), as well as a measurement of brain surface area. These values provide a second type of measurement of brain surface characteristics.

RESULTS: VALIDATION OF BRAINPLOT AND BRAINMAP

The opportunity to obtain a highly faithful visual representation of the surface of the human brain *in vivo* represents a new frontier in neuroscience/neuroimaging. Although the images appear visually quite realistic, the image processing involved in generating these images requires a number of steps that could produce distortion that could lead to misrepresentation of actual anatomy. Therefore, validation studies are imperative. No single validation study can perfectly assess the precision or accuracy of the measurements produced. Consequently, several different approaches to validation were used, involving postmortem tissue and *in vivo* human imaging data. These validation studies suggest that BRAINPLOT and BRAINMAP do provide useful indices of brain surface anatomy.

Postmortem Studies. Two postmortem brains were scanned, using the spoiled grass sequence described above, while immersed in water inside a plastic container. The scans obtained were of high quality; they were then volume rendered using BRAINBLAST, subjected to analysis with BRAINPLOT, and revisualized again using the combined information derived from the curvature indices and the spatial location information through BRAINMAP. A photograph of one brain, as well as the volume rendering from BRAINBLAST and revisualization from BRAINMAP, are shown in Fig. 4. As Fig. 4 indicates, the surface anatomy visualized through BRAINBLAST closely resembles the actual brain, as does the anat-

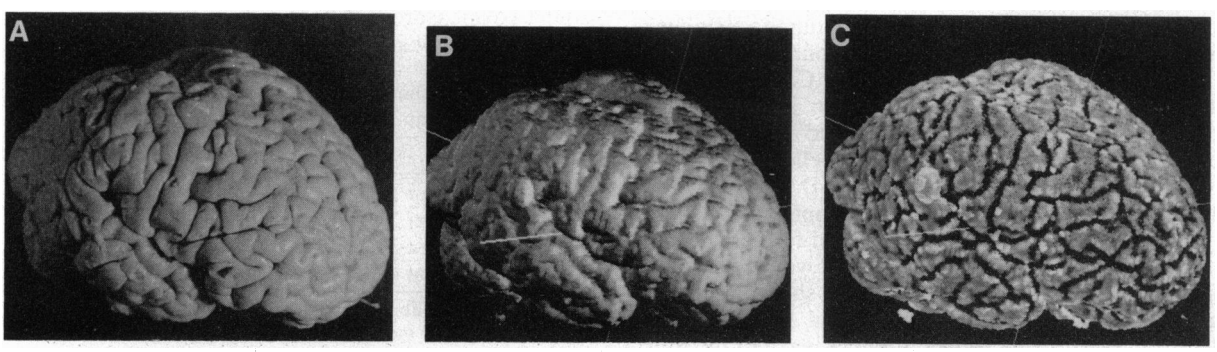

FIG. 4. A postmortem brain (*A*), which has been scanned using MR and reconstructed three-dimensionally using BRAINBLAST (*B*); the reconstructed image has been analyzed using the BRAINPLOT/BRAINMAP methods and revisualized (*C*). Note the close resemblance in sulcal/gyral anatomy. Note also that the BRAINBLAST image is unevenly lit, due to the use of lighting models, while the sulci and gyri have more even shading in the BRAINMAP visualization.

omy visualized through BRAINMAP, confirming that both BRAINBLAST and BRAINMAP provide an accurate representation of brain surface anatomy.

Phantom Studies. An additional validation check was made by using computer-generated phantoms. The phantoms were simply described mathematical functions, such as a sine wave bent into a circle and given a pixelated surface. They were designed in order to create a simple simulation of the problems that might arise in the differentiation between normal and atrophic brains. An example of the sine wave figure is shown in Fig. 3 and described as "Atrophic." If the method is valid, the statistical moments should be able to distinguish this object from the scalloped object in Fig. 3, referred to as "Normal." Specifically, the distribution of the scalloped object's curvature indices should be more skewed since there are many points of gentle convexity (moderate positive values) and a few severely obtuse concavities (large negatively signed values). For each of the two shaped objects, normal and atrophic, 1100 phantoms were manufactured that varied in amplitude, radius, and number of cycles. These objects were easily distinguished by the moments using a nonparametric canonical discriminant analysis [likelihood ratio = 0.149; $F = 3126.26$; degrees of freedom (df) = 4, 2195; $P < 0.0001$]. This analysis was able to correctly identify 2180 phantoms of the 2200 as being normal or atrophic.

We also used the phantoms to see how well the statistical moments related to the amplitude, number of cycles, and number of cycles in a given arc. These parameters, although grossly oversimplified, correspond to surface complexity in the human brain. Each of these parameters affected the moments with distinctive patterns. For instance, increasing amplitudes affected all the moments, while increasing cycles modified the centeredness, variance, and kurtosis but left the skew unchanged. These results confirm that the method is robust to detecting expected differences in simple geometric figures.

Human Data. The most meaningful check on the validity of these methods involves human data. Specifically, can they provide quantitative estimates of differences in brain surface structure that are consistent with recognizable brain pathology?

In this aspect of the study, we determined whether the quantitative measurements generated by BRAINPLOT and BRAINMAP could distinguish between brains with normal surface anatomy and brains with a surface that appears atrophic. Twenty-eight subjects were evaluated using MR scans from our pool of >200 subjects who have been studied with a T1 weighted 1.5-mm spoiled grass sequence. Fourteen subjects were selected who had surface anatomy identified as atrophic, while the other 14 had normal surface anatomy. Those considered atrophic were rated on a scale of 0–5, analogous to the CERAD scale [P. Davis, M. Gado, A. Kumar, L. Gray, K. Maravilla, F. Jolesz, M. Albert, and A. E. George (1989) CERAD neuroimaging protocol for the assessment of Alzheimer's disease (Consortium to Establish a Registry for Alzheimer's Disease, St. Louis)] and a consensus rating was made by two clinicians (N.C.A. and M.F.). The atrophy scale applied was based on anchor points defined by a locally developed photographic atlas; its interrater reliability has been assessed and is excellent. The mean atrophy rating for this group was 3.87 (SD = 0.26). The subjects in the normal group had a mean atrophy rating of 1.7 (SD = 0.01). The two groups were matched for gender.

The data comparing the subjects with and without atrophy are summarized in Table 1. The two groups show significant differences in three of the four statistical moments. As predicted from the schema shown in Fig. 3, each of the four statistical moments is greater in the normal than in the atrophic brains. The normal brains have a nonsignificant trend to a larger mean (moment one), indicating that they are more highly curved, perhaps reflecting the fullness of healthy gyri. The normal brains also have a significantly greater variance; this may occur because the normal brain has a greater variety and complexity of invaginations, while disease has caused the atrophic brains to regress to the mean. The normal brains also have a significant increase in skewness, which is in the negative direction; this may reflect an increase in surface complexity which is due to a greater degree of enfolding or invagination. The normal brains also differ in the fourth moment, kurtosis; this difference may reflect the fact that the curvature indices of the atrophic brain have become more "gaussian" in their overall distribution (i.e., akin to the regression to the mean as reflected in moment two), while the normal brain remains more "non-gaussian" statistically, reflecting a greater diversity of surface pattern.

Table 1. Atrophy vs. nonatrophy groups: Statistical moments of the curvature indices

	Atrophy		Nonatrophy			
	$\bar{x}$	SD	$\bar{x}$	SD	t	P
Moment 1 (mean)	6.82	1.81	8.78	3.36	−1.92	0.07
Moment 2 (variance)	27.03	1.84	30.56	3.13	−3.63	0.001
Moment 3 (skewness)	2.68	0.97	3.91	1.78	2.27	0.03
Moment 4 (kurtosis)	8.19	0.96	9.95	1.95	−3.02	0.007

Because these statistical moments are mathematically related to one another (i.e., constitute a polynomial function) and are also highly correlated with one another, we conducted a second analysis in which we used logistic regression in order to explore the unique contribution of the four moments to the differences. Data in this analysis have been corrected for overall head size, since the distribution of the curvature indices is influenced by the object's size (i.e., a Ping-Pong ball has a more tightly curved surface than does a basketball). The results are summarized in Table 2, which indicates that moment three is providing the strongest contribution to the findings and could alone be used to differentiate the two groups. Sensitivity and specificity of the prediction was acceptable (71% and 64%, respectively). The biological meaning, as well as the clinical utility, of measuring these moments requires further exploration in other types of samples. In comparisons between other groups (e.g., males vs. females), it is conceivable that other moments could make a stronger contribution. Until these methods receive further study using a variety of data sets, both univariate and multivariate approaches to analysis should be evaluated.

In a second analysis, we examined the ability of the technique to classify subjects as atrophic vs. normal, using the two measures generated from BRAINMAP: number of surface voxels classified as convex (having a positive curva-

Table 2. Contribution of the four moments to predicting atrophy group membership

	χ^2	P
Moment 1 (mean)	2.94	0.087
Moment 2 (variance)	13.22	0.0003
Moment 3 (skewness)	0.42	0.515
Moment 4 (kurtosis)	0.14	0.138

Maximum likelihood based on logistic regression. Overall model includes the four moments plus estimated curvature. Overall χ^2 for the four moments = 16.711; df = 4; $P < 0.002$. These maximum likelihood χ^2 values are the tests for unique contributions from a hierarchical model. The estimated curvature is not a simple linear head size correction but involves an expected curvature, which is a linearized transform of radius.

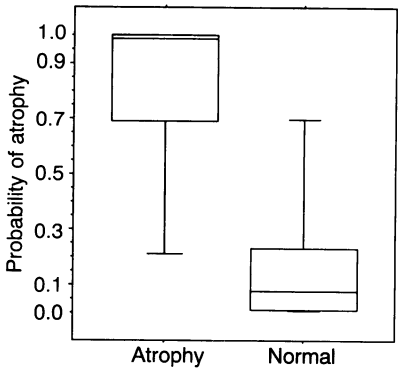

FIG. 5. Box plots showing differences between normal and atrophic groups. Box plots indicate distributions of the estimated probabilities that a brain is atrophic using the logistic regression of the four moments. Solid boxes mark off middlemost 50% of the distribution with the center horizontal lines at the medians. Vertical lines extend through the upper and lower quartile of the distribution.

ture index) and number classified as concave (having a negative curvature index). These were combined with an estimate of brain surface area based on brain volume; the volumetric measure was transformed to an area estimate (i.e., raised to the 2/3 power) to provide a comparable metric. In this case, simple t tests also indicate highly significant differences between the groups (for positive C_a, $t = 5.437$; df = 26; $P < 0.00001$; for negative C_a, $t = 4.735$; df = 26; $P < 0.0001$). We again applied logistic regression; the two groups are well separated, with very little overlap ($\chi^2 = 24.55$; df = 2; $P < 0.000005$). The sensitivity and specificity of these measures (86% for both) is superior to that of the moments. An analysis visually displaying the separation of the two groups using box plots is shown in Fig. 5; the two groups are clearly well differentiated with almost no overlap. These results suggest that the technique may have clinical utility for identifying and quantifying the presence of atrophy.

DISCUSSION

Strengths of the Method. The large amount of anatomic information generated through MR presents a conceptual and methodological challenge. The newer sequences, which provide very detailed anatomic data, require analytic techniques that are relatively rapid, automated, and simple. Manual techniques are far too labor intensive (and subject to individual rater variation or error) to study large samples. While postmortem studies by nature involve the intensive investigation of small samples, a major strength of MR as a neuroanatomic tool is its ability to collect data noninvasively in large samples of informative individuals.

BRAINPLOT and BRAINMAP provide a method for adapting to these challenges. First, they require very little user intervention. Second, they generate quantitative estimates of brain surface features. While the applications of these quantitative estimates are still in a developmental phase, the above application to atrophic versus nonatrophic brains suggests that the approach is robust to detecting significant anatomical differences.

Third, through BRAINMAP, an alternative and innovative visual representation of brain surface is produced. Most current techniques that apply volume/surface rendering to do three-dimensional visualization of the brain surface rely on "lighting models," which display the sulci and gyri by illuminating them from various directions in order to produce highlights and shadows. Application of lighting models has a variety of limitations, since the surface appearance of the brain will vary depending on the number and direction of the lights; furthermore, manipulations such as rotation or tracing on the surface are also affected by lighting; sulci and gyri will assume different appearances as they are moved around in relation to the lights. The image of brain surface generated through BRAINMAP carries its lighting model within it: the curvature indices are assigned a grey scale value that reflects the degree of curvature. The resulting image is a highly faithful rendering of the brain surface.

Future Directions. BRAINPLOT and BRAINMAP have a variety of potential applications. These techniques should be useful for the study of variations in sulcal/gyral patterns in various cerebral subregions. For example, given the relatively late development of the prefrontal cortex, one might anticipate a different degree of complexity in that area, as compared to other brain regions. A second and related application is the examination of correlates between surface patterns and a variety of disease states. For example, one would anticipate that developmental anomalies such as pachygyria should be readily detectable with this technique. A third application is the examination of the correlates between surface anatomy and cognitive abilities. For example, the relationship between sulcal/gyral surface characteristics and general intelligence can be explored.

This research was supported in part by National Institute of Mental Health Grants MH31593, MH40856, and MHCRC 43271; the Nellie Ball Trust Fund; and Research Scientist Award MH00625.

1. Schwartz, J. M., Aylward, E., Barta, P. E., Tune, L. E. & Pearlson, G. D. (1992) *Am. J. Psychiatry* **149,** 1195–1198.
2. Vannier, M. W., Brunsden, B. S., Hildebolt, C. F., Falk, D., Cheverud, J. M., Figiel, G. S., Perman, W. H., Kohn, L. A., Robb, R. A., Yoffie, R. L. & Bresina, S. J. (1991) *Radiology* **180,** 479–484.
3. Cline, H. E., Lorensen, W. E., Souza, S. P., Jolesz, F. A., Kikinis, R., Gerig, G. & Kennedy, T. E. (1991) *J. Comput. Assisted Tomogr.* **15,** 344–351.
4. Robb, R. A. & Barillot, C. (1989) *IEEE Trans. Med. Imaging* **8,** 217–226.
5. Rusinek, H., Mourino, M. R., Firooznia, H., Weinreb, J. C. & Chase, N. E. (1989) *Radiology* **171,** 269–272.
6. Tiede, U., Hoehne, K. H., Bomans, M., Pommert, A., Reimer, M. & Wiebecke, G. (1990) *IEEE Comput. Graphics Applic.* **10,** 41–53.
7. Toga, A. (1990) in *Three-Dimensional Neuroimaging* (Raven, New York).
8. Runge, V. M., Gelblum, D. Y. & Wood, M. L. (1990) *Neuroradiology* **32,** 356–366.
9. Bomans, M., Höhne, K. H., Tiede, U. & Riemer, M. (1990) *IEEE Trans. Med. Imaging* **9,** 177–183.
10. Levin, D. N., Hu, X., Tan, K. K. & Galhotra, S. (1989) *Radiology* **171,** 277–280.
11. Pommert, A., Tiede, U., Wiebecke, G. & Höhne, K. H. (1990) in *First Conference on Visualization in Biomedical Computing* (Inst. Elec. Electron. Eng., Piscataway, NJ), pp. 19–26.
12. Folley, J., van Dam, A., Feiner, S. & Hughes, J. (1990) in *Computer Graphics: Principles and Practice* (Addison-Wesley, Reading, MA), 2nd Ed., pp. 729–731.
13. Ono, M., Kubic, S. & Abernathy, C. (1990) *Atlas of the Cerebral Sulci* (Thieme, New York).
14. Goldman, P. S. & Galkin, T. W. (1978) *Brain Res.* **152,** 451–485.
15. Goldman-Rakic, P. S. (1980) *Prog. Brain Res.* **53,** 1–19.
16. Goldman-Rakic, P. S. & Rakic, P. (1984) in *Cerebral Dominance: The Biological Foundation*, ed. Geschwind, N. & Galaburda, A. M. (Harvard Univ. Press, Cambridge, MA), pp. 179–192.
17. Zilles, K., Armstrong, E., Schleicher, A. & Kretschmann, H.-J. (1988) *Anat. Embryol.* **179,** 173–179.
18. Eggers, R., Haug, H. & Fischer, D. (1984) *J. Hirnforsch.* **25,** 129–139.
19. Haug, H. (1987) *Am. J. Anat.* **180,** 126–142.
20. Pakkenberg, B. (1992) *Acta Neurol. Scand. Suppl.* **137,** 20–33.
21. Zeki, S., Watson, J. D. G., Lueck, C. J., Friston, K. J., Kennard, C. & Frackowiak, R. S. J. (1991) *J. Neurosci.* **11,** 641–649.
22. Jouandet, M. L., Tramo, M. J., Herron, D. M., Hermann, A., Lostus, W. C., Bazell, J. & Gazzaniga, M. S. (1989) *J. Cogn. Neurosci.* **1,** 88–117.
23. Andreasen, N. C., Cohen, G. C., Harris, G., Cizadlo, T., Parkkinen, J., Rezai, K. & Swayze, V. W., II (1992) *J. Neuropsych. Clin. Neurosci.* **4,** 125–133.
24. Andreasen, N. C., Cizadlo, T., Harris, G., Swayze, V., O'Leary, D. S., Cohen, G., Ehrhardt, J. & Yuh, W. T. C. (1993) *J. Neuropsych. Clin. Neurosci.* **5,** 121–130.
25. Cohen, G., Andreasen, N. C., Alliger, R., Arndt, S., Kuan, J., Yuh, W. T. C. & Ehrhardt, J. (1992) *Psychiatr. Res. Neuroimaging* **45,** 33–51.
26. Talairach, J. & Tournoux, P. (1988) *Co-Planar Stereotaxic Atlas of the Human Brain* (Thieme, New York).